ORIGINAL ARTICLE

Induced shear in reinforced concrete beams with synthetic aggregate

Cisalhamento induzido em vigas de concreto armado com agregado sintético

Willian Jorge Rodrigues Amaral[a] (iD)
Dênio Ramam Carvalho de Oliveira[a] (iD)

[a]Universidade Federal do Para – UFPA, Grupo de Análise Experimental de Estruturas e Materiais – GAEMA, Belém, PA, Brasil

Abstract: The increasing aluminum production demands larger volumes of bauxite residue (BR) to be stored in the Amazon region. There are millions of tons of waste without reuse but with high potential for use in civil construction as artifacts or components for concrete. Due to the significant consumption of coarse aggregates for concrete, there is the possibility of producing synthetic aggregate (SA) from bauxite residue, containing high levels of residue (70%, 80% and 90%), maintaining satisfactory levels of resistance and durability. To evaluate this new product, two beams were made with conventional aggregate (gravel) and the others with SA. For the evaluation of the shear strength, friezes were made to fix the failure surface, aiming to reduce the influences of the arch action on the shear strength, inducing the failure in the brittle section. The friezes presented inclinations of 30° or 45°, according to the calculation models of the Brazilian code for concrete structures. All beams were subjected to bending test until failure. The results showed that the SA has potential for use in reinforced concrete structures, presenting a similar performance to the conventional aggregate. The results also showed the preponderance of tensile when the *a/d* ratio increases, evidencing the greater contribution of the coarse aggregate with the increase of the strut inclination.

Keywords: shear, beams, reinforced concrete, bauxite residue, Amazon.

Resumo: A crescente produção de alumínio demanda crescentes volumes de resíduo da bauxita (RB) a serem estocados na região Amazônica. São milhões de toneladas de resíduo sem reaproveitamento, mas com elevado potencial para utilização na construção civil como artefatos ou insumos para concretos. Devido ao significativo consumo de agregados graúdos para concretos, tem-se a possibilidade de produção de agregado sintético (AS) de RB, contendo elevados teores do resíduo (70%, 80% e 90%), mantendo-se níveis satisfatórios de resistência. Para avaliar o novo produto, foram confeccionadas duas vigas com agregado convencional (brita) e outras duas com AS. Para a avaliação da resistência ao cisalhamento, foram feitos frisos (entalhes em angulações pré-definidas) para fixação da superfície de ruptura, visando reduzir as influências do efeito de arco na absorção do esforço cortante, induzindo a ruptura por cisalhamento na seção. Os frisos apresentaram inclinação de 30° e 45°, de acordo com os modelos de cálculo recomendados pela norma brasileira. As vigas foram submetidas a ensaios de flexão até a ruptura. Os resultados mostram que o AS apresenta potencial para uso em estruturas de concreto armado, com desempenho similar ao agregado convencional. Os resultados mostram ainda, a preponderância da tração diagonal à medida que a relação *a/d* aumenta, evidenciando a maior contribuição do agregado por efeito de engrenamento com o aumento da inclinação da biela.

Palavras-chave: cisalhamento, vigas, concreto armado, resíduo de bauxita, Amazônia.

1 INTRODUCTION

The extraction of alumina through the digestion of bauxite in caustic soda, at high temperature and pressure, still generates highly toxic residues that contaminate the environment [1]. In this processing, an insoluble residue known as Red Mud (RM), or Bauxite Residue (BR) is generated in large quantities. The production of 1 ton of alumina generates around 2 ton of BR and 1 ton of CO_2 [2]. Currently, around 150 million tons (Mton) of BR are produced per year, of which around 2% to 3% are reused or recycled in a productive way [3], [4]. From the Brazilian production of BR, 6.1 Mton, 4.9 Mton are deposited in the Amazon [5]. Although not particularly toxic, BR offers risks to the environment due to its large volume and its reactivity. According to the latest technology, part of its moisture is removed, and the BR is stacked in specially constructed impermeable bins [6].

The production of coarse aggregate has been one of the productive ways of using BR. It is known that the shear strength is intrinsically linked to the resistance, shape and diameter of the coarse aggregate, which is responsible for resisting shear stresses by the effect known as aggregate interlock. Therefore, the synthetic aggregate of BR can be used in reinforced concrete structures, as long as its performance is satisfactory. The increase in its diameter improves the stress transfer mechanisms, increasing the shear resistance through aggregate interlock, due to the perimeter extension through which the critical crack will have to travel around the aggregate. This mechanism makes a significant contribution to shear strength in reinforced and prestressed concrete beams.

Experimental tests have indicated that between 33% and 50% of the total shear force can be transferred by the aggregate interlock [7]. With increasing crack opening due to increased load, the ability to resist shear stress through aggregate interlock is reduced. In these stages, the main resistant mechanism is the longitudinal reinforcements, which offer resistance by the dowel action. The faces of the crack tend to slip due to shear stresses, causing a relative transverse displacement in the longitudinal reinforcement, mobilizing this reaction force [8]. According to Manzoli et al. [9] the dowel action can significantly contribute to the transfer of shear forces, mainly in the load stages close to or after the ultimate load, when the shear stresses are no longer resisted by the aggregate.

2 RESEARCH SIGNIFICANCE

The BR is composed by potentially toxic chemicals due to the processing of bauxite for the extraction of aluminum. The high concentration of sodium hydroxide is responsible for the corrosive potential for vegetation and contamination of groundwater, due to the presence of heavy metals, such as iron, aluminum and titanium oxides, which may compromise the supply of drinking water. The possibility of using coarse BR aggregates in reinforced concrete structures will mitigate the environmental impact generated by the waste, giving it the potential for use in the composition of concrete as an alternative to conventional aggregate. Previous studies have already used BR in the composition of concrete [6]. However, there are no studies in the literature on the performance of these aggregates from the point of view of shear strength. Therefore, the present work aims to evaluate the viability of using these coarse aggregates in reinforced concrete beams when subjected to shear forces in the ultimate limit state.

3 MATERIALS AND EXPERIMENTAL PROGRAM

3.1 Methodology

Four (4) reinforced concrete beams were made with the same span and cross section, with friezes inclined of 30° or 45° (Table 1) and two types of coarse aggregate, natural and synthetic.

Table 1. Beams main variables.

Beam code	$\theta°$	Coarse Aggregate	$D_{máx}$ (mm)
B30C	30	Conventional	9.5
B30S	30	Synthetic	9.5
B45C	45	Conventional	9.5
B45S	45	Synthetic	9.5

The beams were tested under the four-point test system or Stuttgart loading scheme (Figures 1 and 2), mounted on the reaction slab of the Civil Engineering Laboratory (LEC) of the Federal University of Pará (UFPA), as shown on Figure 3. The beams present an isostatic condition, supported on rollers on reaction blocks, supporting the load applied perpendicularly to its longitudinal axis, in the middle of the span, on the upper face of the beam, through a bi-supported

metallic rail for load distribution in two points simulating a simple and pure flexure situation, coupled to the reaction frame fixed to the slab. The load application device consists of a manually operated hydraulic cylinder with load capacity of 1000 kN, driven by a hydraulic pump, under a load cell with a capacity of 1000 kN and precision of 1 kN, connected to a digital load indicator. The loading steps were about 5 kN.
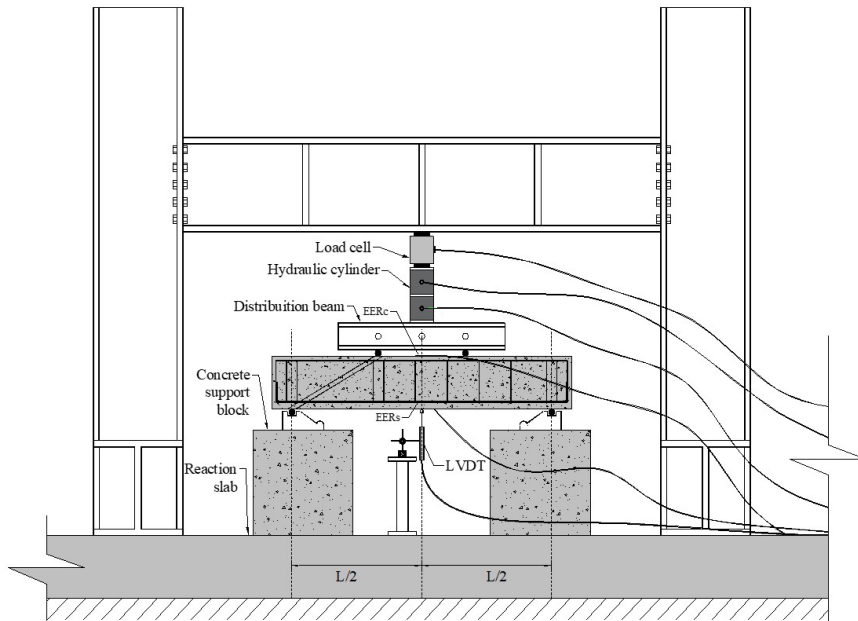

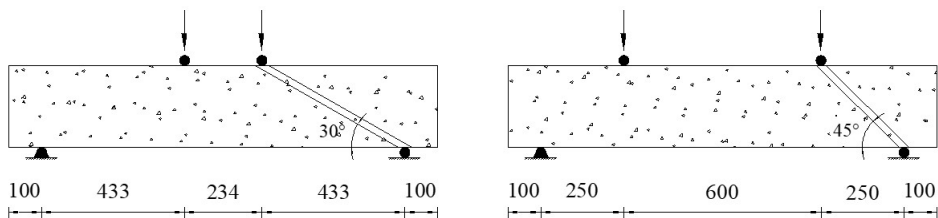**Figure 1.** Four-point test system, front view.

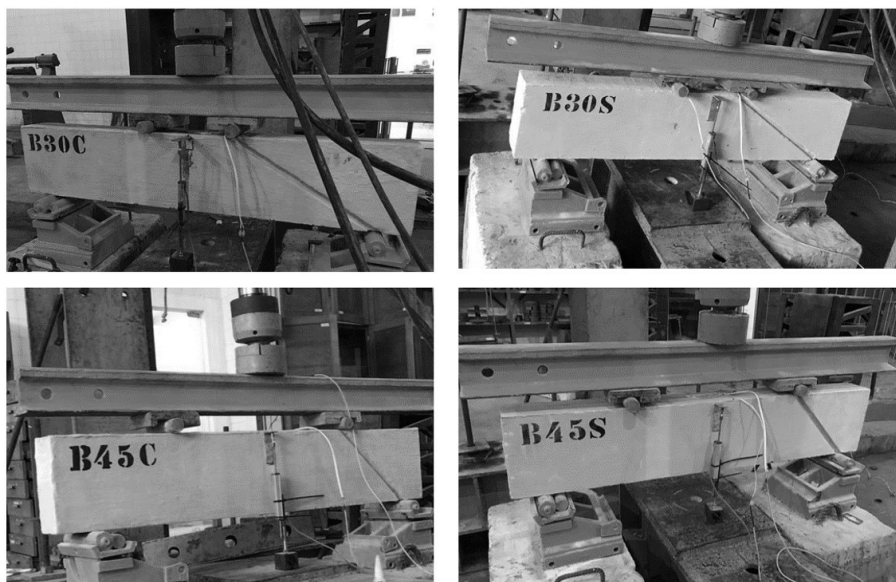**Figure 2.** Loading position and friezes.

Figure 3. Beams ready to be tested.

3.2 Monitoring

The monitoring of the longitudinal reinforcement strains was carried out using electrical resistance strain gauges (EER,s) by Excel Sensors, with a grid dimensions of (3 x 3) mm – model PA-06-125AA-120L, which were fixed to the side surface of reinforcement ($\emptyset/2$), positioned at half the span ($l/2$) in the region of pure flexure and maximum bending moment (Figures 4 and 5). For the concrete, electrical resistance strain gauges (EERc) by Excel Sensors were also used, with a grid measuring (51 x 2) mm – model PA-06-201BA-120L, fixed on the beams' top surface, previously prepared and smoothed using epoxy adhesive. Only the midspan ($l/2$) was monitored, exactly at the midwidth (Figure 6).
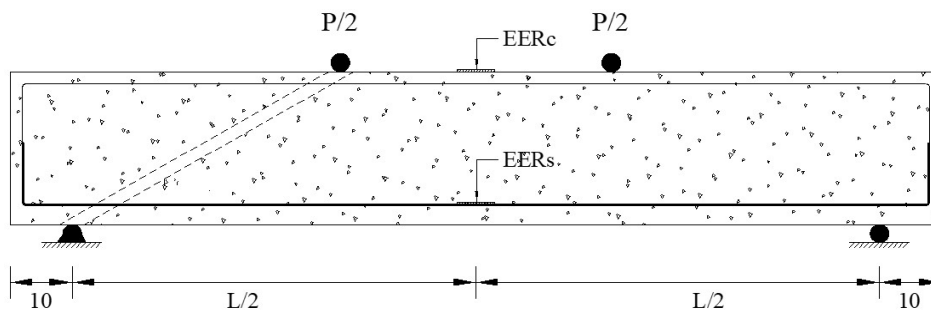

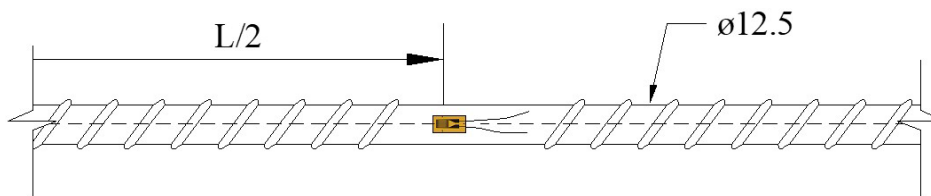**Figure 4.** Concrete and steel strains monitoring.

Figure 5. Strain gage at midheight of the flexural reinforcement bar (EERs)
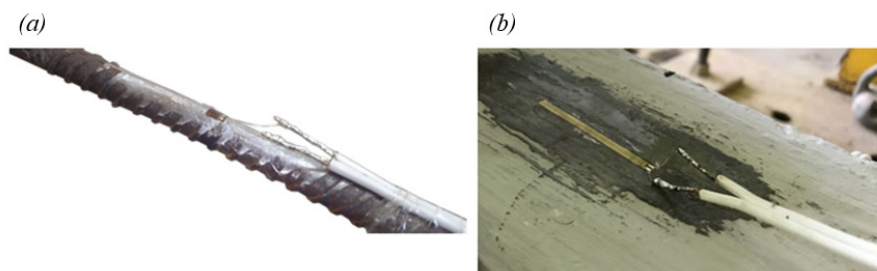

Figure 6. Strain gages at (a) flexural reinforcement and (b) concrete.

3.3 Failure surface definition (frieze)

The purpose of using the friezes was to weaken the concrete section at a predetermined angle, inducing shear failure in this inclined section. In the present study, the angles 45° and 30° refer to the inclinations of the struts based on the truss theory. The beams present *a/d* ratio equal to 1.0 and 1.7 for the inclinations of the friezes to 45° and 30°, respectively, and the manifestation of the arch action is expected. This phenomenon is negligible for beams with *a/d* ratio greater than 2.5 [10] or when the *a/h* ratio is greater than 3 [11], where *h* is the height of the beam. This effect makes the failure surface angle of the tensioned diagonal difficult to predict, since after the appearance of inclined cracks a complex redistribution of stresses occurs, making the mechanisms responsible for the transfer of the shear force difficult to measure [12]. However, with the use of friezes, the influence of the arch action is significantly reduced, causing the critical shear crack to occur at the pre-established angle, generating shear failure in the weakened section, making it possible to evaluate the shear strength without this effect.

Figures 7 and 8 show the influence of the frieze in the trajectory of the main stresses where the difference in behavior of the angle of rotation responsible for the maximum and minimum stresses is observed. Considering points A, B and C, for a beam without frieze (Figure 7), the rotation angle of the element that leads to the main stresses is variable along the diagonal formed between the load application point and the supports, presenting itself in the form $\theta_1 < \theta_2 < \theta_3$,

respectively for points A, B and C, due to the influence of the arch action. For a beam with frieze (Figure 8), the same inclination of the angle referring to the maximum and minimum stresses is observed along the diagonal formed by the support and the load application point, $\theta_1 = \theta_2 = \theta_3$. Therefore, for points A, B and C, respectively, there is the same inclination of the strut. Unlike a beam without friezes, the plane is fixed at a pre-established angle, so that the actions of the arch action are reduced significantly, causing the maximum compression and tension to occur in this plane.
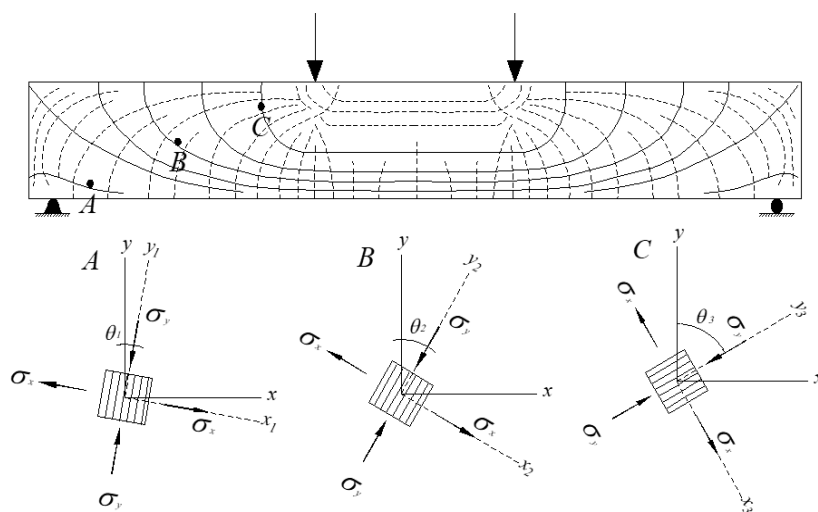
Figure 7. Trajectory of the main stresses in beam without frieze.
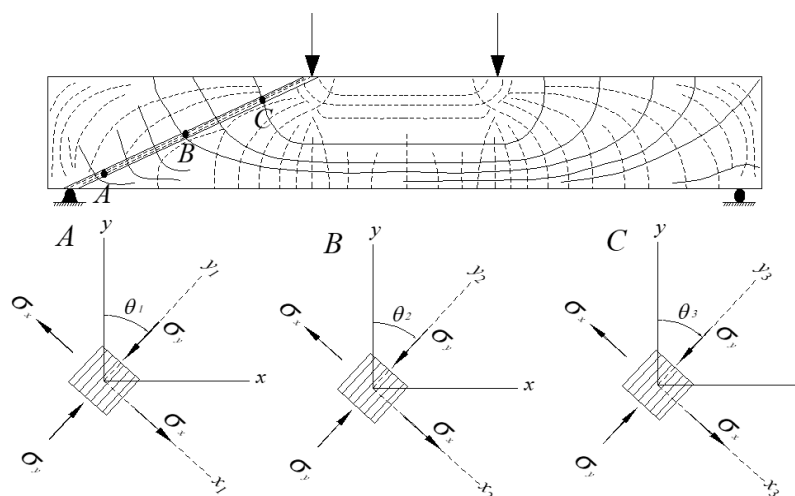
Figure 8. Trajectory of the main stresses in beam with frieze.

3.4 Beams characteristics

The beams presented cross section of (120 x 250) mm, 1300 mm length and 1100 mm span. Although b_w be 120 mm and the cover 20 mm, the ultimate load is predicted considering the width b_w to 90 mm, due the depth of friezes, equals to 15 mm. The longitudinal reinforcements were designed to resist bending and the shear failure would occur before yielding along the frieze's length (Figures 9 and 10). The molds were made using resinous wood with a thickness of 10 mm and the friezes, executed from the shape itself with wood strips on the referred inclinations (Figure 11), so that there was no need for post concreting cutting.
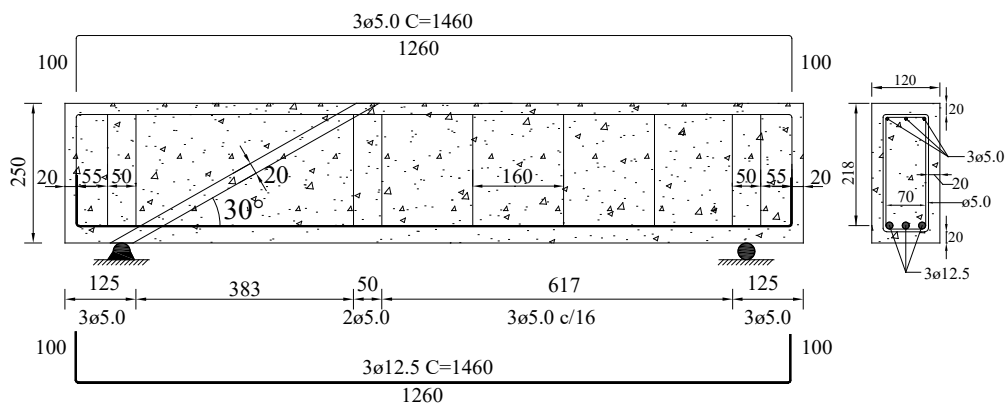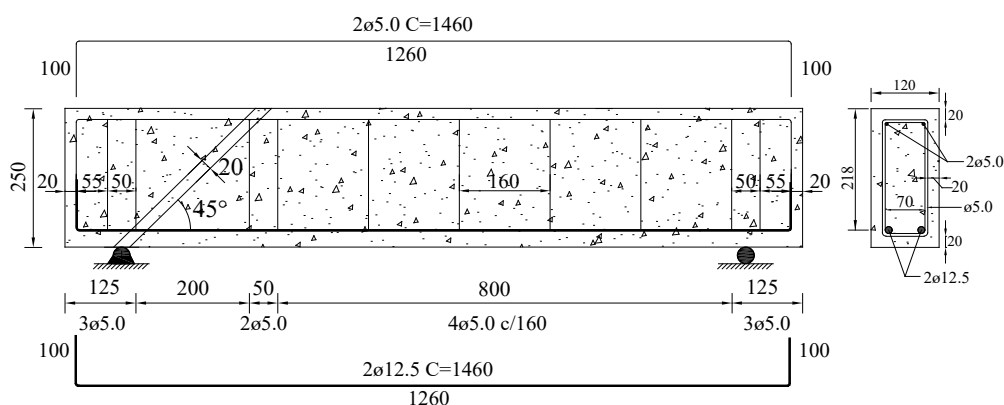
Figure 9. Beams with friezes inclined of 30°.

Figure 10. Beams with friezes inclined of 45°.
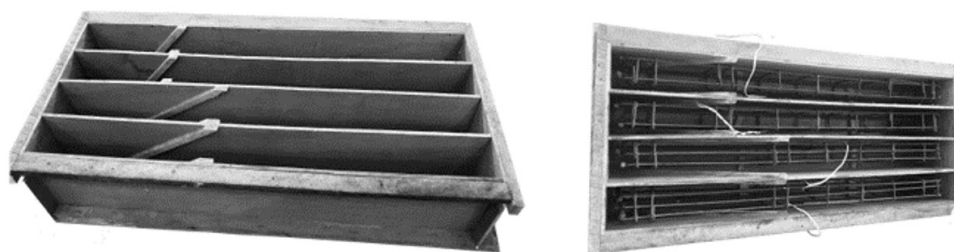
Figure 11. Beams molds.

3.5 Synthetic aggregate properties

The synthetic aggregate (SA) consists of three materials: bauxite residue, silica and clay (Table 2). The material is produced by mixing and then burning these materials at a temperature of 1200°C for a period of 3 hours. By varying the proportions of these materials, SA-90, SA-80 e SA-70samples are obtained, whose objective is to increase the aggregate production scale and, consequently, the consumption of bauxite residue.

Table 3 presents some properties of SA-80 and the chemical composition of the BR was provided by HYDRO Alunorte (Table 4). It is important to emphasize that the toxicity of SA was not evaluated. The final composition of synthetic aggregate (Table 5) shows that the material is essentially composed of iron (37%), aluminum (16%) and silicon (29%), showing that the aggregate holds the main proportions of the BR.

Rev. IBRACON Estrut. Mater., vol. 17, no. 3, e17303, 2024

6/14

Table 2. Synthetic coarse aggregate properties (70%, 80% and 90% of BR).

Sample	BR	Silica	Clay	Specific weight	Temperature	Time
	(%)	(%)	(%)	(g/cm³)	(°C)	(h)
SA-90	95 – 90	0 - 5	5	> 2.0	1200	3
SA-80	85 – 80	10 - 15	5	> 1.5 e < 2.0	1200	3
SA-70	75 – 70	20 - 25	5	< 1.5	1200	3

Table 3. Test results related to the synthetic coarse aggregate with 80% of BR.

Method	Absorption test [13]	Solubilization test [14]	Abrasion *Los Angeles* test [15]	Shape index test [16]
Sample	Absorption	pH	Loss to abrasion	Index
	(%)		(%)	
SA-80	8.12 < 10	8.96 > 5	11 < 50	1.77 < 3

Table 4. BR chemicals composition.

Composition	Content
	(%)
Al_2O_3	21.27
SiO_2	17.72
Fe_2O_3	34.31
TiO_2	6.89
Na_2O	9.25
CaO	1.22
LOI	8.11

Table 5. SA-80 chemicals composition.

Composition	Content
	(%)
Na_2O	7.68
MgO	0.56
Al_2O_3	16.90
SiO_2	29.30
SO_3	0.20
K_2O	0.32
CaO	1.02
TiO_2	5.22
Cr_2O_3	0.10
MnO	0.15
Fe_2O_3	37.00
ZrO_2	1.05
Pr_6O_{11}	0.11
Nd_2O_3	0.25

3.6 Mix and proportion of materials

The concretes followed a relationship of (1:4), one part of cement to four of fine and coarse aggregates. The workability was specified in order to simulate the usual construction situations, considering a slump test equal to 100±20 mm. To reduce the porosity and improve the compressive resistance, the addition of active silica was used.

Rev. IBRACON Estrut. Mater., vol. 17, no. 3, e17303, 2024

7/14

The list of materials for the dosage of concrete followed the proportion [1:1.5:2.5:0.4], both for conventional concrete and for concrete with SA, resulting in the materials expressed in the Table 6. Figure 12 shows the natural and synthetic aggregates. Figure 13 shows that both concretes reached similar workability, allowing concreting in usual situations.

Table 6. Concrete admixture.

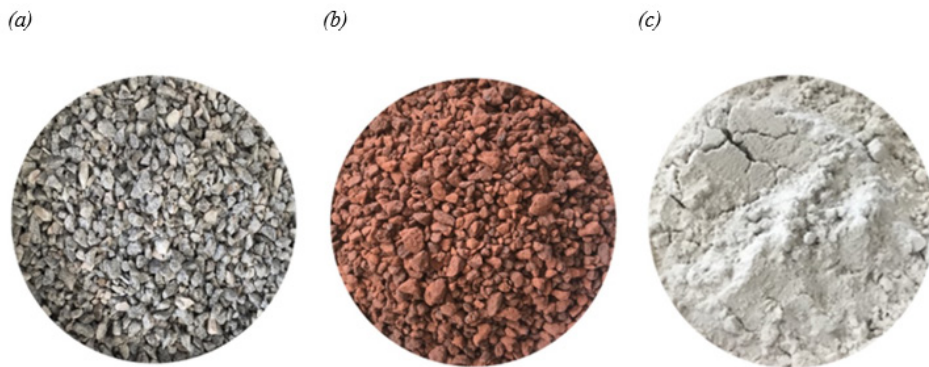| Material	B45S e B30S	B45C e B45S
Portland Cement CP II – F	50 kg	50 kg
Thin sand	75 kg	75 kg
Granite gravel	-	125 kg
Synthetic aggregate of BR	125 kg	-
Water	19.7 kg	19.7 kg
Powerflow addictive	300 mL	300 mL
Active silica	500 g	500 g
Workability	100 ± 20	100 ± 20

Figure 12. Coarse and fine aggregates used in concretes: (a) gravel, (b) SA and (c) sand.

Figure 13. Slump test for the concretes (a) conventional and (b) SA.

4 RESULTS AND DISCUSSION

4.1 Materials characterization

The characteristic compressive strength was obtained according to Brazilian normative criteria [17]. Nine cylindrical specimens with a nominal diameter of 100 mm and a height of 200 mm were molded and tested (Figure 14). The average values for compressive strength f_{cm} of the conventional and SA concrete were, respectively, 47.4 MPa and 41.3 MPa, according to Table 7.
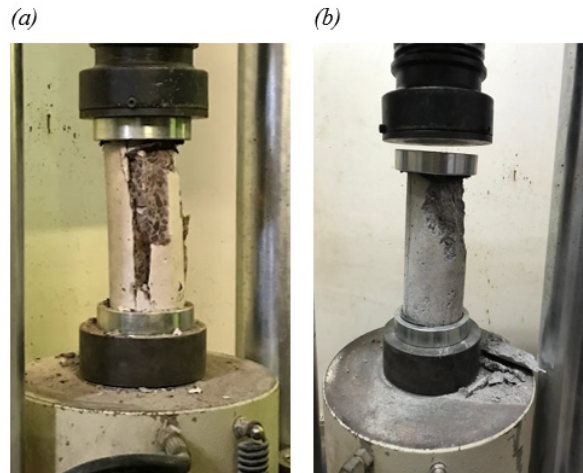
(a)   *(b)*

Figure 14. Compressive strength test for concretes with (a) SA, and (b) granitic gravel aggregate.

Table 7. Concretes compressive strength results.

CP	Conventional aggregate	Synthetic aggregate
	(MPa)	(MPa)
CP-I	47.7	40.2
CP-II	47.3	42.1
CP-III	47.1	41.6
f_{cm}	47.4	41.3

As in the compressive strength test, the Modulus of Elasticity tests also followed the normative criteria of the Brazilian standard [18], using the same geometry of the specimens used for the uniaxial compressive strength test (Figure 15). The average results of modulus of elasticity (E_{cm}) were to 36.8 GPa for conventional concrete and 27.8 GPa for concrete with synthetic aggregate, as presented in Table 8.
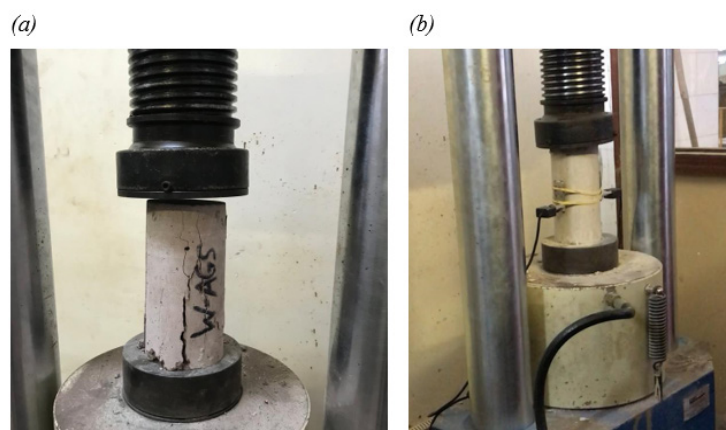
(a)   *(b)*

Figure 15. Modulus of Elasticity test for concretes with (a) SA, and (b) granitic gravel aggregate.

Table 8. Modulus of elasticity results for concretes.

CP	Conventional aggregate (GPa)	Synthetic aggregate (GPa)
CP-I	35.4	28.4
CP-II	38.3	27.2
E_{cm}	36.8	27.8

4.2 Deflections

The results of the LVDT reading provide the vertical displacements for each load step, observed over a distance of $\ell/2$, being ℓ the span length. The beams have the same moment of inertia, making concrete the only variable in bending stiffness. $(E \cdot I)$ due to the composition of the material, differentiated by the type of coarse aggregate – synthetic BR and conventional granitic gravel. For the beams in this work, the limit deflection is 4.4 mm, for a span of 1,100 mm, according to sensory acceptability criteria [19]. The maximum deflection observed for beams with a frieze to 30° (B30C and B30S) were 2.5 mm and 3.8 mm, respectively. For the beams with a frieze to 45° (B45C and B45S) the observed values were 4.3 mm and 5.3 mm, respectively (Table 9, Figures 16 and 17). Beam B45S showed excessive deflection and exceeded the Brazilian code limit. The relationship between the flexural reinforcement yield load (P_{flex}) and the ultimate load P_u makes clear the brittle failure mode by shearing. Figure 18 shows the evolution of the displacements as the load increases.

Table 9. Deflection results.

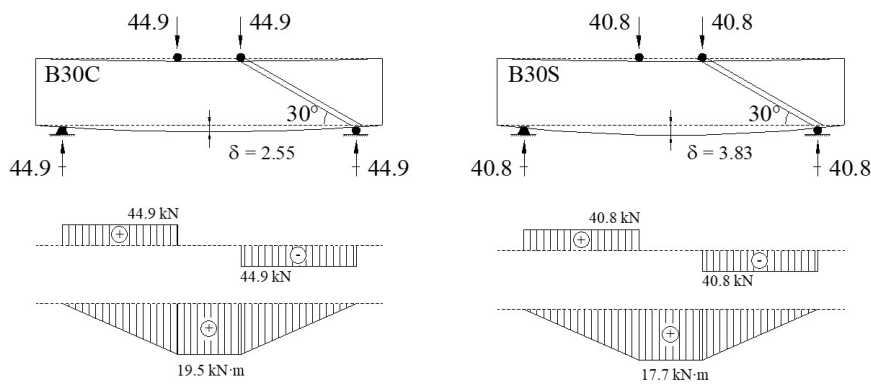| Beam code	ρ (%)	f_c (MPa)	P_u (kN)	P_{flex} (kN)	P_{flex}/P_u	δ (mm)	$l/250$ (mm)
B30C	1.4	47.4	89.4	162.8	1.81	2.5	4.4
B30S	1.4	41.3	81.7	161.4	1.97	3.8	4.4
B45C	0.9	47.4	156.9	196.8	1.25	4.3	4.4
B45S	0.9	41.3	139.1	194.4	1.38	5.3	4.4

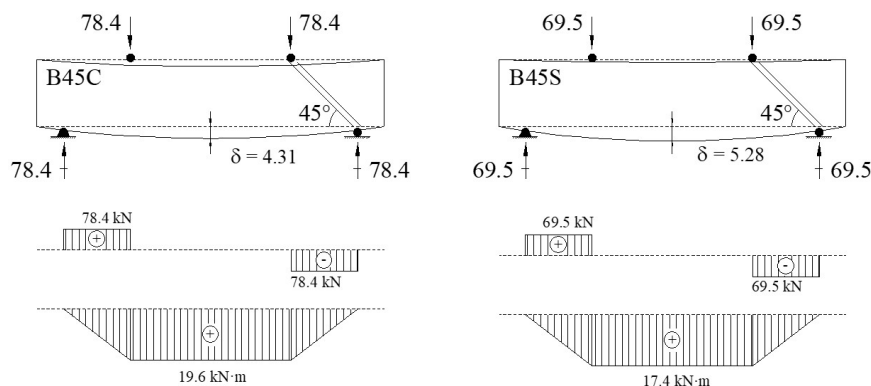**Figure 16.** Shear force and bending moment diagrams for beams with friezes inclined of 30°.

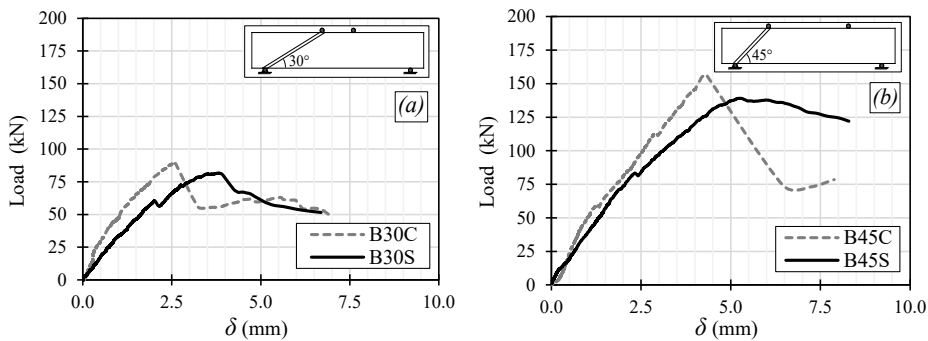**Figure 17.** Shear force and bending moment diagrams for beams with friezes inclined of 45°.

Rev. IBRACON Estrut. Mater., vol. 17, no. 3, e17303, 2024

10/14

Figure 18. Diagram load-deflection for the beams with friezes inclined of (a) 30° and (b) 45°.

4.3 Strains

The Stuttgart test system generates normal tensile and compressive stresses without shearing interference between the loading points, and the maximum stresses are located at the top (compression) and bottom (tensile) surfaces of the midspan cross section. Figures 19 and 20 show the evolution of tensile and compressive strains as the loading increases. The longitudinal reinforcement strains (Figure 19) show that none of the bars monitored by the EERs exceeded the yield point, equal to 2.38 ‰ for the CA-50 steel, used in this reinforcement. The tensile strain values for beams B30C and B30S were 1.01 ‰ and 1.22 ‰, respectively, while for beams B45C and B45S were 0.88 ‰ and 0.69 ‰, respectively.

The concrete strains (Figure 20) were below the limit strain for concrete crushing (3.5 ‰) until failure by shear in all beams, varying the strain according to the stiffness of each element, as seen in the load-strain diagrams. The values observed for beams B30C and B30S were 0.54 ‰ and 0.61 ‰, while for B45C and B45S, 2.47 ‰ and 2.34 ‰, respectively. The Figures 21 and 22 show that the beams with frieze to 30° presented higher tensile strains in the flexural reinforcements that those of the beams B45C and B45S. However, the opposite behavior is observed for concrete, where a greater demand is observed for the beams with frieze to 45° in relation to the beams with 30° inclination.
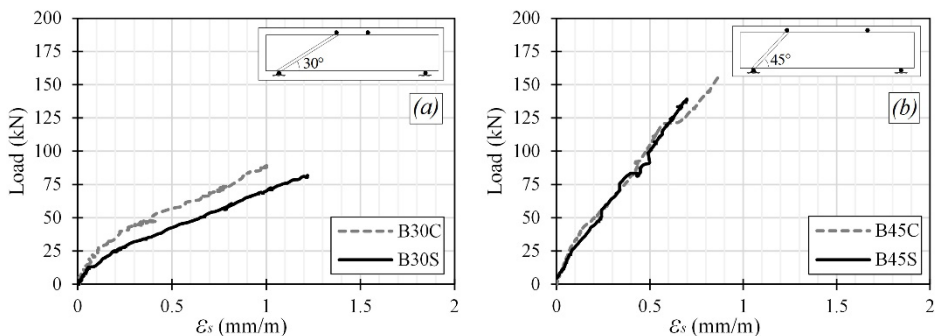

Figure 19. Flexural reinforcement strains for beams with frieze to (a) 30° and (b) 45°.
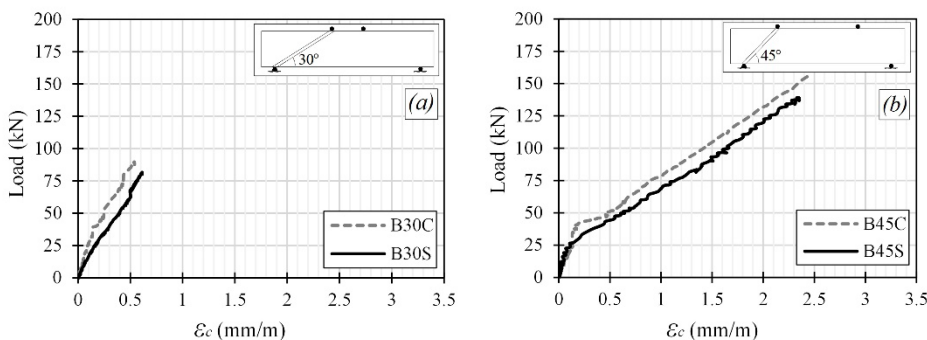

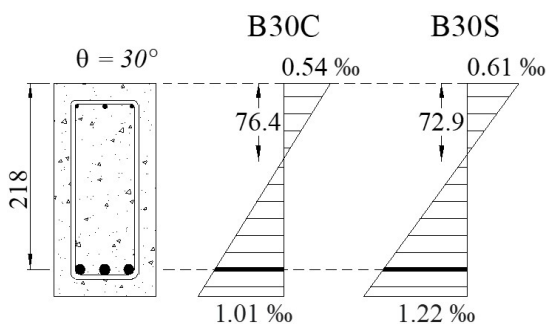**Figure 20.** Concrete strains for beams with frieze to (a) 30° and (b) 45°.

Rev. IBRACON Estrut. Mater., vol. 17, no. 3, e17303, 2024

11/14

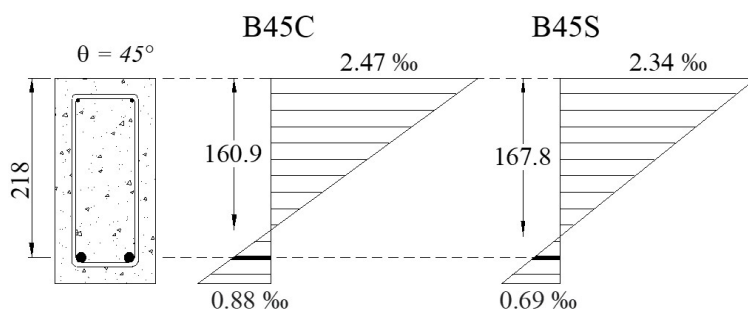**Figure 21.** Strain diagram for beams with frieze to 30°.

Figure 22. Strain diagram for beams with frieze to 45°.

4.4 Failure and cracking patterns

As expected for shear failures, the B30C beam presented brittle failure, with an abrupt drop in the load intensity right after the first shear crack appearance, around 77% of the ultimate load. On the other hand, the B30S beam showed greater number of cracks, starting around 49.0 kN (around 60% of the ultimate load) in the length between loading points. As the loading increased, the cracking became significant and began to show an inclination towards the load application points, a typical configuration of a shear crack (Figures 23 and 24). The ultimate loads of 89.4 kN and 81.7 kN were recorded for beams B30C and B30S, respectively. Beams with frieze to 45° showed greater resistance compared to 30° frieze ones due to the aggregate interlock contribution to shear resistance associated to the higher inclination of the strut. The beams with 30° friezes presented lower failure loads due to the predominance of diagonal tensile and, consequently, the smaller contribution of the aggregate interlock. Beam B45C presented more cracks than B30C, both presenting the first cracks between the loading points, as well as the B45S, with about 56% of the failure load. The flexural cracks in beam B45S occurred with 74 kN loading. The cracking patterns for B45S and B45C beams were similar, starting in the central region without the influence of shear and spreading towards the beams' ends and tilting to loading application points. All beams presented shear failure surface at the inclined cross section between friezes, as estimated. The ultimate load for beams B45C and B45S were 155.4 kN and 147.4 kN, respectively.
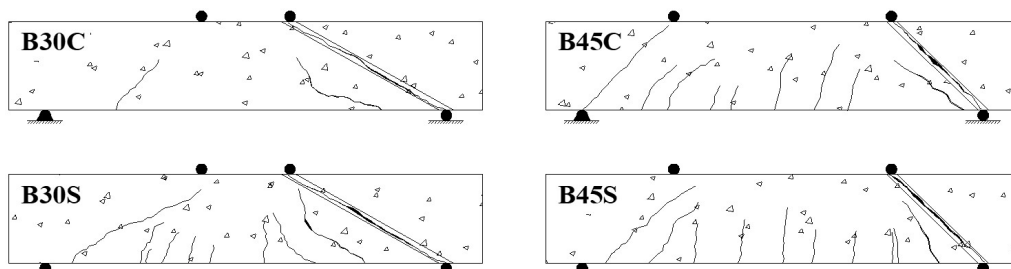

Figure 23. Beams cracking patterns.

Rev. IBRACON Estrut. Mater., vol. 17, no. 3, e17303, 2024

12/14

Figure 24. Beams after failure

The theoretical failure load (P_{NBR}) was defined according to the calculation models from the Brazilian design code. The model I for beams with a 45° frieze and two branch stirrups spaced of $s = 200$ mm (Equation 1), and model II for beams with 30° frieze and without transverse reinforcement (Equation 2). The Brazilian code proved to be accurate, according to Table 10, once the friezes allowed experimental results free from arch action. For beams with 30° frieze the P_u/P_{NBR} relationship was one, and when the aggregate interlock effect is more preponderant (45°frieze), this relationship presented greater variance but lesser than 10%.

$$P_{NBR} = 0.35 \cdot f_c^{\frac{2}{3}} \cdot b_w \cdot d + 2.52 \cdot \frac{A_{sw}}{s} \cdot f_{yw} \cdot d \tag{1}$$

$$P_{NBR} = 0.35 \cdot f_c^{2/3} \cdot b_w \cdot d \tag{2}$$

Table 10. Theoretical and experimental results.

Beam code	a/d	ε_c (‰)	ε_s (‰)	P_{flex} (kN)	P_u (kN)	P_{NBR} (kN)	P_u/P_{NBR}	P_{flex}/P_u	Failure
B30C	1.7	2.47	0.88	162.8	89.4	90.2	0.99	1.81	Shear
B30S	1.7	2.34	0.69	161.4	81.7	82.2	0.99	1.97	Shear
B45C	1.0	0.54	1.00	196.8	156.8	155.4	1.01	1.25	Shear
B45S	1.0	0.61	1.22	194.4	139.1	147.4	0.94	1.39	Shear

5 CONCLUSIONS

The present work evaluated the shear behavior of reinforced concrete beams without transverse reinforcement and using in its composition the synthetic aggregate of bauxite residue. The synthetic aggregates were produced from the mixture of bauxite residue, clay and silica, subsequently burned at 1,200° C for a period of 3 hours. Four beams were made and friezes were used to stablish a failure surface at angles of 30° and 45°, according to the truss theory, aiming to eliminate the influences of the arch action, since all beams presented $a/d < 2.5$. From the methodology presented by the experimental program and the behavior observed in the tests, the following conclusions were possible.

• The synthetic aggregate of bauxite residue is suitable for use in structural concrete, obtaining satisfactory results in all normative criteria for coarse aggregate. In addition, the material also presented workability conditions similar to conventional concrete for the same dosage, with the same materials;

• The mechanical performance of concrete beams with synthetic aggregate showed satisfactory results in terms of shear strength. The conventional concrete beams showed superior results of 8% and 11% for beams with friezes to 30° and 45°, respectively. However, the greater compressive resistance of the conventional concrete must be highlighted;

• The Brazilian standard proved to be assertive for predicting the ultimate shear load, when the influence of the arch action is drastically reduced. For beams with 30° frieze, the calculation model practically gives a single result. For the 45° frieze beams, this model showed greater variance, with safety and acceptable values;

• The beams with friezes inclined of 30° resisted less than the 45° frieze ones, evidencing the contribution of the coarse aggregate interlock, where it was experimentally observed that the greater the ratio *a/d*, the smaller will be the contribution due to aggregates interlock in the resistance of the beams;

• The use of friezes to induce shear failure proved to be efficient because the failure of all beams occurred in the predetermined failure surface (30° or 45°).

ACKNOWLEDGEMENTS

REFERENCES

[1] S. Rai, K. Wasewar, J. Mukhopadhyay, C. K. Yoo, and H. Uslu, "Neutralization and utilization of red mud for its better waste management," *Arch. Environ. Sci*, vol. 6, pp. 5410, 2012.

[2] C. M. Carter, H. A. van der Sloot, D. Cooling, A. van Zomeren, and T. Matheson, "Characterization of untreated and neutralized bauxite residue for improved waste management," *Environ. Eng. Sci.*, vol. 25, no. 4, pp. 475–488, 2008.

[3] K. Evans, E. Nordheim, and K. Tsesmelis 'Bauxite residue management', in *Light Metals 2012*, C. E. Suarez, Ed., Cham: Springer, 2012, pp. 61–66. https://doi.org/10.1002/9781118359259.ch11.

[4] K. Evans "Success and challenges in the management and use of bauxite residue", in *Bauxite Residue Valorization and Best Practices Conferences*, 2015. https://conference2015.redmud.org/wp-content/uploads/2015/10/Ken-EVANS-secure.pdf (accessed Feb. 27, 2023).

[5] D. R. C. de Oliveira and C. R. C. Rossi, "Concretes with red mud coarse aggregates," *Mater. Res.*, vol. 15, no. 3, pp. 333–340, May 2012, http://dx.doi.org/10.1590/S1516-14392012005000033.

[6] F. A. Botelho, "Estudo da influência da adição de óxido de cálcio e óxido de magnésio na neutralização e estabilização da alcalinidade do resíduo de bauxita através da reação com dióxido de caBRono," Doctoral dissertation, UFPA, Belém, Brasil, 2017.

[7] M. Lachemi, K. M. A. Hossain, and V. Lambros, "Shear resistance of self-consolidating concrete beams — experimental investigations," *Can. J. Civ. Eng.*, vol. 32, no. 6, pp. 1103–1113, Dec 2005., http://dx.doi.org/10.1139/l05-066.

[8] C. G. Nogueira, "Desenvolvimento de modelos mecânicos, de confiabilidade e de otimização para aplicação em estruturas de concreto armado," Doctoral dissertation, EESC USP, São Carlos, Brasil, 2010. https://doi.org/10.11606/T.18.2010.tde-29062010-113700.

[9] O. L. Manzoli, J. Oliver, G. Diaz, and A. E. Huespe, "'Three-dimensional analysis of reinforced concrete members via embedded discontinuity finite elements Análise tridimensional de elementos estruturais de concreto armado via elementos finitos com descontinuidades incorporadas," *Rev. IBRACON Estrut. Mater.*, vol. 1, pp. 58–83, 2008.

[10] J. G. MacGregor and J. K. Wight, *Reinforced Concret: Mechanics and Design*, 6th ed. Hoboken: Pearson, 2012.

[11] F. Leonhardt and E. Monnig, *Construções de Concreto*, 2nd ed. Stuutgart: Editora Interciência, 1973.

[12] R. C. Fenwick and P. Thomas, "Mechanisms of shear resistance of concrete beams," *J. Struct. Div.*, vol. 94, no. 10, pp. 2325–2350, Oct 1968, http://dx.doi.org/10.1061/JSDEAG.0002092.

[13] Associação Brasileira de Normas Técnicas, *Determinação da Densidade e da Absorção de Água*, ABNT NBR 16917:2021, 2021.

[14] Associação Brasileira de Normas Técnicas, *Resíduos sólidos - Classificação*, ABNT NBR 16917:2021, 2004.

[15] Associação Brasileira de Normas Técnicas, *Ensaio de Resistência ao Impacto e à Abrasão Los Angeles*, ABNT NBR 16974:2022, 2022.

[16] Associação Brasileira de Normas Técnicas, *Determinação do Índice de Forma pelo Método do Paquímetro - Método de ensaio*, ABNT NBR 7809:2019, 2019.

[17] Associação Brasileira de Normas Técnicas, *Concreto - Ensaio de Compressão de Corpos de Prova Cilíndricos*, ABNT NBR 5739:2018, 2018.

[18] Associação Brasileira de Normas Técnicas, *Concreto - Determinação do Módulo Elasticidade à Compressão*, ABNT NBR 8522:2008, 2008.

[19] Associação Brasileira de Normas Técnicas, *Projeto de Estruturas de Concreto - Procedimento Design of Concrete Structures-Procedure*, ABNT NBR 6118:2014, 2014.